nature communications

Article

https://doi.org/10.1038/s41467-025-56554-x

Mélange dehydration and melting beneath South Sandwich Islands arc

Received: 22 March 2024

Accepted: 22 January 2025

Published online: 07 February 2025

Check for updates

Yunchao Shu[1,2,3,4] ✉, Sune G. Nielsen[1,3,5] ✉, Veronique Le Roux[3,5], Danielle Santiago Ramos[1,6], Jerzy Blusztajn[1,3], Maureen Auro[1], Phil T. Leat[7,8] & Tristan J. Horner[1,9]

Mechanisms regulating material transfer from subducted slabs to arc magmas remain debated, centered on metasomatized mantle wedge interactions versus mélange mobilization at the slab-mantle interface. The South Sandiwch Islands arc offers a unique setting to distinguish between these models due to the significant barium isotope contrast between altered oceanic crust and sediments, the latter displaying unusually light barium isotope compositions compared to the global sediment range. Here we show substantial barium isotope variations coupled with invariant strontium isotope ratios in arc lavas, consistent with mélange mobilization beneath the arc. Northern arc lavas display a broader range of barium isotope values than expected from slab inputs, suggesting barium isotope fractionation during slab material transport, potentially driven by phengite-related barium retention within the mélange. Notably, sediments, rather than altered oceanic crust, emerge as the dominant source of barium in arc lavas. While a comparison of barium isotope data from four additional arcs indicates mantle wedge metasomatism remains visible in several cases, mélange mobilization is consistent with available data across all of these subduction zones.

Subduction zones are the loci of mass transfer between the Earth's surface and its deep interior. They play a major role in Earth's heat budget and have a significant impact on long-term climate. Additionally, subduction zones are the sites of valuable ore deposit creation and pose one of the most serious natural risks to humanity through major earthquakes and volcanic eruptions. Geochemical evidence has shown that material released from the subducted slab, primarily sediments, hydrothermally altered oceanic crust (AOC), and perhaps serpentinite, plays a significant role in generating arc lavas and imparting distinct chemical signatures to arc volcanism[1–3]. However, significant debate exists regarding the exact mechanisms that control this mass transfer[4–9], which has important implications for the division of slab material between Earth's surface and deep mantle.

Some trace element ratios (e.g., Sr/Nd, U/Nb, Ba/Th) in primitive arc lavas fall well outside the range of subducted components. This discrepancy suggests that the mechanisms involved in transferring these components from the subducting slab to arc volcanoes must include a means of fractionating trace element ratios beyond the values observed for discrete subduction zone inputs. Such fractionation can occur via the involvement of fluids from—or partial melts of—slab material[4,10,11]. The fluid-mobile element barium (Ba) exhibits significant enrichment in arc lavas compared to mid-ocean ridge basalts (MORBs)[2,10]. Consequently,

[1]NIRVANA (Non-traditional Isotope Research for Various Advanced Novel Applications) Laboratories, Woods Hole Oceanographic Institution, Woods Hole, MA, USA. [2]Laoshan Laboratory, Qingdao, China. [3]Department of Geology and Geophysics, Woods Hole Oceanographic Institution, Woods Hole, MA, USA. [4]Department of Earth Sciences, The University of Hong Kong, Pokfulam, Hong Kong. [5]Centre de Recherches Pétrographiques et Géochimiques, CNRS, Nancy, France. [6]Department of Marine and Coastal Sciences, Rutgers University, New Brunswick, NJ, USA. [7]British Antarctic Survey, Cambridge, UK. [8]School of Geography, Geology and the Environment, University of Leicester, Leicester, UK. [9]Department of Marine Chemistry and Geochemistry, Woods Hole Oceanographic Institution, Woods Hole, MA, USA. ✉e-mail: yshu@hku.hk; sune.nielsen@univ-lorraine.fr

it has been hypothesized that Ba enrichment in arc lavas reflects the input of a Ba-rich component derived from the subducted slab. The source of the Ba enrichment has been traced by normalizing its concentration to that of elements with similar compatibility such as La or Th. High Ba/La and Ba/Th ratios in arc lavas are often inferred to reflect the addition of fluid from AOC, because experiments in which fluids were equilibrated with basaltic ocean crust indeed showed that Ba is substantially more soluble in aqueous fluids than Th and La over temperature and pressure ranges relevant to subduction zones (600–1000 °C; 4–6 GPa)[12,13]. However, sedimentary Ba concentrations are highly variable (100–10,000 μg/g), because the mineral barite ($BaSO_4$) controls the Ba budgets of many marine sediments[14]. Some individual sediment horizons rich in barite display extremely high Ba concentrations (up to 10,000 μg/g), and extremely high Ba/Th and Ba/La that can exceed the highest ratios observed in arc lavas[14]. Hence, the ultimate source of Ba enrichments in arc lavas remains uncertain. Recent advancements in Ba isotope studies have revealed the potential to distinguish the source of Ba enrichments in subduction zones[15–18], thereby providing insight into the mechanisms of mass transfer under arcs. This potential is premised on the different components exhibiting distinct $\delta^{138/134}$Ba (Ba isotope compositions, whereby $\delta^{138/134}\text{Ba}\,(‰) = 1000 \times (^{138}\text{Ba}/^{134}\text{Ba}_{\text{sample}} \div {}^{138}\text{Ba}/^{134}\text{Ba}_{\text{standard}} - 1)$, where the standard is National Institute of Standards and Technology (NIST) Ba Standard Reference Material (SRM) 3104a). For example, studies have shown that sediments exhibit $\delta^{138/134}$Ba of ≈−0.1 to +0.1‰[15,19–21] and AOC with $\delta^{138/134}\text{Ba} = +0.20 \pm 0.10‰$[19,22], which differ from those of the fresh MORBs ($\delta^{138/134}\text{Ba} \approx -0.04$ to +0.15‰)[19,23,24].

Models of mass transfer processes from slab to mantle wedge and then to arc magmas fall into two broad categories, at least from an isotope mass balance perspective. The first model proposes that individual components of the incoming slab melt and/or dehydrate before mixing and/or reacting with the mantle wedge[2,5,25,26]. The second model suggests that rock mixing and fluid metasomatic processes occur at the slab-top, leading to the formation of mélanges that then melt and/or dehydrate and participate in arc magma generation[9,27–29]. We, therefore, hypothesize that these two categories of arc magma generation processes should have distinct consequences for predicted Ba isotope relationships. In the metasomatized mantle wedge models, water-rich fluids primarily come from dehydration reactions of AOC or deeply seated serpentinites[1,2,5], whereas sediments and sometimes AOC at the top of the slab produce partial melts[11,26,30–32]. These fluids and sediment/AOC melts then metasomatize the overlying mantle wedge, which subsequently melts to form arc magmas. In the mélange models, components of the mantle wedge, sediments, and AOC mix via shearing and fluid metasomatism at the slab–mantle interface. The newly formed and hydrated mélange then partially melts and/or dehydrates, either at the slab-top or in buoyant diapirs[29]. However, we stress that there is currently no geochemical means to distinguish between a slab-top and diapir origin of magmas derived from mélange materials.

In this study, geochemical co-variations for Ba and radiogenic Sr isotopes (Fig. 1) will be used to distinguish between the two model categories. Within the framework of the first model, serpentinites typically have very low Ba and Sr concentrations and the hydrothermal reactions that cause serpentinization do not add significant Ba and Sr[33–35], thus serpentinite-derived fluids are not able to perturb the Ba and Sr budget of subduction fluids. The AOC and sediments have much higher Ba concentrations as well as Ba isotope values that can be

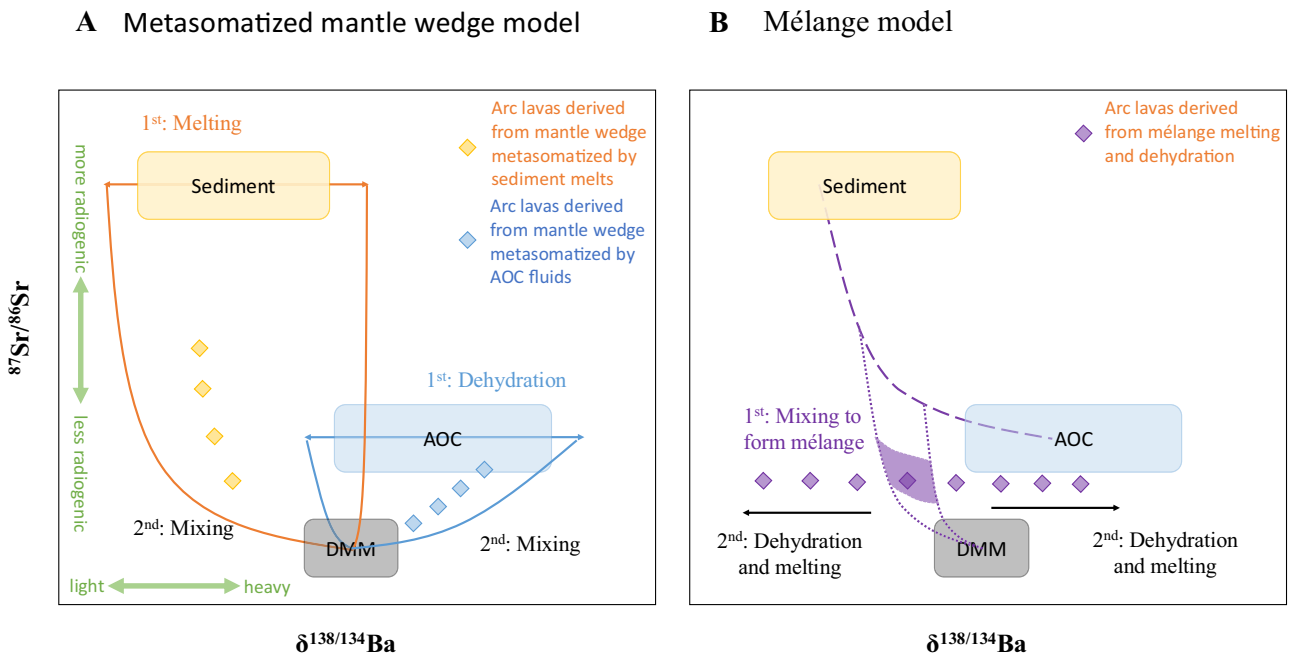

Fig. 1 | Schematic illustration of Ba isotopes vs Sr isotopes to distinguish the two different end-member models of slab material transport in subduction zones. A In the metasomatized mantle wedge model, sediment and AOC (yellow and blue boxes, respectively), which both potentially show fractionated Ba isotope characteristics upon melting and dehydration, respectively (orange and blue horizontal lines extending from boxes), mix with the mantle wedge to form arc magmas. Orange and blue lines represent mixing lines between mantle wedge and sediment melts and between mantle wedge and AOC fluids, respectively. Yellow and blue diamonds represent arc magmas produced by the mixing of sediment melts and AOC fluids, respectively, with DMM. **B** In the mélange model, sediment, AOC, and the mantle wedge physically mix to form hybrid mélange rocks with a Sr isotope ratio determined by the relative proportions of the components that formed the mélange. The mélange subsequently melts and/or dehydrates to form arc magmas with fractionated Ba isotope signatures. A mixing line between sediment and AOC (purple dashed line) is shown. Purple dotted lines represent mixing lines between the mantle wedge and subducted slab components with different proportions of sediment and AOC. The purple area indicates mélange compositions. Purple diamonds represent arc magmas generated from mélange melting and dehydration. Data sources of the DMM[19,23,24,43,91], sediment[14,15,19–21], and AOC[19,22,92–94] are all from literature (see text for details).

https://doi.org/10.1038/s41467-025-56554-x

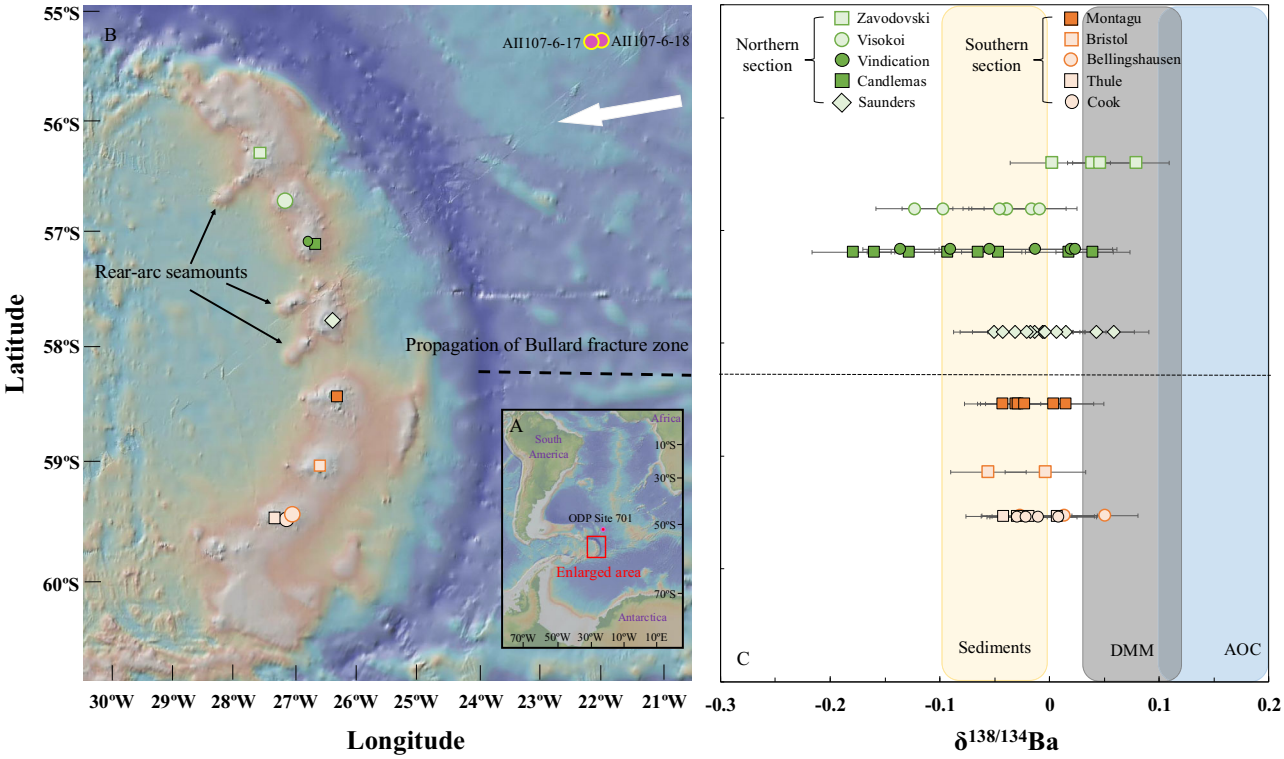

Fig. 2 | Location of South Sandwich Islands (SSI) subduction zone and Ba isotope characteristics in the SSI arc. A Location of SSI arc and surrounding areas. **B** Map of the SSI arc volcanoes. Also shown is the location of two sediment cores from which samples were analyzed in this study to constrain the composition of the sediment input to the arc. The black dashed line represents the propagation of the Bullard fraction zone, which divides the SSI arc into northern and southern sections. The approximate plate motion direction is represented by a white arrow[60]. **C** Regional variations in Ba isotope systematics with latitude along the SSI arc. Also shown are the Ba isotope compositions of the DMM ($\delta^{138/134}$Ba = +0.03 to +0.12‰)[19,23,24], AOC ($\delta^{138/134}$Ba = +0.20 ± 0.10‰)[19,22], and sediments (this study) (see text for details). Error bars associated with the $\delta^{138/134}$Ba values represent 2 standard deviations (SD) of sample reproducibility. The image of the landform was made with GeoMapApp 3.6.10 (www.geomapapp.org)/CC BY/CC BY[95]. Source data are provided as a Source Data file.

distinct from the upper mantle[15,19,22], and thus could serve as significant sources of isotopically anomalous Ba in arcs. Dehydration reactions of hydrous minerals in subducted slab materials have been inferred to fractionate Ba isotopes based on results for high-pressure metamorphic rocks[36,37], and AOC typically exhibits Ba isotope values similar to or higher than upper mantle[19,22]. Therefore, a positive correlation between Ba and Sr isotope values in arc magmas, or variable Sr isotope values with mantle-like Ba isotope values, would likely suggest the involvement of AOC-derived hydrous fluids[16,18]. Conversely, sediments typically exhibit Ba isotope values similar to or lighter (lower $\delta^{138/134}$Ba) than the upper mantle[15,19–21,38]. Thus, the involvement of sediment melts would produce a negative correlation between Ba and Sr isotopes in arc magmas, or variable Sr isotope compositions with mantle-like or variable Ba isotope values. Schematically, it is expected that mixtures of the mantle wedge with discrete sediment melts or AOC-derived fluids should produce magmas that fall along sub-vertical mixing lines, with variation in Sr isotopes and limited covariation of Ba isotopes (Fig. 1A). On the other hand, combined dehydration and melting of mélange rocks has been hypothesized as an alternative mechanism for the generation of arc magmas and can account for both radiogenic isotope and trace element ratio variations observed in arc lavas[4,6,27,39,40]. The mélange layer located at the slab–mantle interface may consist of several kilometer-thick zones of physically mixed, sheared, and metasomatized sediments, AOC, and serpentinized mantle[27,28,41]. Therefore, some heterogeneities will be expected in mélange rocks, as also ubiquitously observed in the field[27,28,42]. However, on the scale of arc magma sources (1–10 km) some of this heterogeneity is likely to attenuate, producing geochemically less variable magmas, which is commonly observed for radiogenic isotope compositions from individual volcanic centers[4]. Given that sediments have Ba concentrations one to three orders of magnitude higher than AOC, and two to four orders of magnitude higher than the mantle[14,19,43], the Ba budget of mélange rocks can principally be dominated by either component depending mostly on Ba content and thickness of subducted sediment. Hydrous fluids derived from the mélange, therefore, are expected to display variable Ba isotope values due to Ba isotope fractionation during dehydration of the hydrous minerals in the mélange together with relatively narrow radiogenic (e.g., Sr, Nd, and Pb) isotope compositions as these are determined by the initial mélange mixing processes. Thus, mélange dehydration and melting are expected to result in horizontal arrays with little variation in Sr isotopes but a range of Ba isotope compositions (Fig. 1B).

Disentangling these models of slab material transport is simplified in arcs where the recycled sediment and AOC components display the largest Ba isotope difference, which has been predicted to occur in the South Sandwich Islands (SSI) arc[15]. The SSI arc is located in the Southern Ocean northeast of the Antarctic Peninsula and consists of 11 islands running 400 km roughly north-south from ~56°S to ~60°S (Fig. 2). The arc has an exceptionally simple structure and is a tectonically primitive intra-oceanic island arc situated on the small Sandwich plate, below which the South American plate is subducting[44]. From north to south along the arc, the volcanic centers include Zavodovski, Visokoi, Candlemas group (Candlemas and Vindication), Saunders, Montagu, Bristol, Southern Thule group (Bellingshausen, Cook, and Thule)[45]. There is no significant influx of continent-derived sediment to the arc-trench system due to its remote location away from pre-existing continental crust, and virtually all of the sediment cover on the subducting plate is subducted[46,47].

Marine barites, which precipitate from the uppermost few hundred meters of the water column[48], exhibit light Ba isotope values due to Ba isotope fractionation during precipitation from seawater with a $\Delta^{138/134}Ba_{barite\text{-}seawater}$ ($=\delta^{138/134}Ba_{barite} - \delta^{138/134}Ba_{seawater}$) of ≈−0.5‰[20,49–51]. The surface waters of the Southern Ocean display the lightest seawater Ba isotope compositions observed to date[51], which should render sediments from this region very light because barites are the main Ba-bearing component of most pelagic sediments[14]. The sediments outboard of the SSI arc are, therefore, expected to exhibit values substantially lighter than the mantle[19,24] and AOC-derived fluids[16,36]. In this respect, arc lavas from the SSI arc are ideal because of the likely distinct Ba isotope signatures for sediments and AOC outboard of the SSI trench. In addition, SSI arc lavas investigated in this study are all basalts or basaltic andesites in which the Ba isotope compositions are unlikely to be pervasively affected by fractional crystallization and/or crustal contamination, as revealed in the Ryukyu and Aleutian arcs[15].

Here we analyzed 63 SSI arc lavas from subaerial locations for Ba isotope compositions. We complement our dataset with trace element and high-precision Sr, Nd, and Pb isotope data for the same samples. We also report elemental and isotope data (Ba, Sr, Nd, Pb) for 9 sediment samples from sediment cores (AII-107-6-17 and AII-107-6-18) collected from the South Atlantic Ocean situated at ~55°S slightly north of the SSI (Fig. 2). These sediments are likely the best available materials representing subducting sediments outboard of the SSI trench as they are more proximal to the SSI arc than those conventionally used (i.e., Ocean Drilling Program (ODP) Site 701 sediments). Our results reveal that systematic variations between Ba isotopes, trace elements, and radiogenic isotope ratios are primarily controlled by dehydration and melting of a mélange underneath the SSI arc, following the predicted relationship outlined in Fig. 1B.

Results

Barium isotope signatures in the SSI arc lavas

Barium concentrations in SSI arc lavas vary from 15.7 to 191 μg/g (Supplementary Table 1), which are higher than those of global MORB glasses[19] and comparable to other arc lavas[15]. The SSI arc lavas display a large range of Ba isotope compositions and include the lightest Ba isotope values in modern arc lavas documented to date[15], with $\delta^{138/134}Ba = -0.18$ to +0.08‰ (Supplementary Table 2). The vast majority of lavas exhibit Ba isotope values of $\delta^{138/134}Ba < 0$‰ (Fig. 2), which is lighter than MORBs ($\delta^{138/134}Ba > 0$‰[19,23,24]). The SSI arc can be divided into northern and southern sections by propagating the long-offset Bullard fracture zone at ~58°S on the South American-Antarctic ridge, which forms the boundary between the South American and Antarctic plates[52,53]. Notably, the northern section of the arc displays more variable Ba isotope compositions than the southern section (Fig. 2). Trace element concentrations, and Sr, Nd, and Pb isotope compositions of the SSI arc lavas are also reported in Supplementary Tables 1 and 2.

Barium isotope characteristics in subducting components

Offshore sediment data from two drill cores are presented (Supplementary Tables 3–5). Though these cores are only about 740 cm and 71 cm long, substantially less than the ~400 m of sediment subducted in the SSI arc[14], the similar lithology and more proximal geographic position to the SSI of these cores than ODP Site 701 (Fig. 2), which has previously been utilized to represent subducted SSI sediments[14,45,54], likely render it a better representation of the Ba isotope input to the SSI arc. This inference is particularly relevant given the gradient in Ba isotope compositions and concentrations between the South Atlantic and Southern Ocean surface seawater from which marine barites precipitate[51]. Most of the Ba in marine pelagic sediments is thought to originate from barite precipitated in surface seawater[14]. Thus, the Ba isotope variations in barite will be the dominant factor controlling the $\delta^{138/134}Ba$ values of the subducting sediment[55]. The Ba isotope compositions of sediments directly outboard of the SSI trench can be inferred based on the systematic relationship between Ba isotope ratios and concentrations in seawater, where lower Ba concentrations are associated with heavier (higher) $\delta^{138/134}Ba$ values[51,55]. Surface seawater between ≈57°S and ≈60°S has similar dissolved Ba concentrations between 75 and 81 nmol/kg, and their isotope compositions display a narrow range between $\delta^{138/134}Ba = +0.3$ and +0.4‰[51,56]. Subducting sediments are, therefore, expected to display a similarly narrow range of Ba isotope values throughout the SSI arc, offset from seawater due to the precipitation of barite. Offshore sediment samples analyzed in this study are siliceous ooze and clay (Supplementary Table 3) and show high and variable Ba concentrations (526–1321 μg/g, Supplementary Table 4) compared to depleted MORB mantle (DMM, ≈0.5 μg/g)[43]. Barium isotope compositions in these sediments exhibit values between $\delta^{138/134}Ba = -0.10$ to 0.00‰ (Fig. 2 and Supplementary Table 5), with a mean, $\delta^{138/134}Ba = -0.05$‰, representing some of the lightest values documented (in comparison to global marine sediments[15,19–21,38]). We also report the trace element and radiogenic isotope systematics (Sr, Nd, Pb) for these sediments in Supplementary Tables 4 and 5. No relationship between Ba concentrations and Ba isotope compositions in the sediments is observed (Supplementary Fig. 1). The sediments in this study display comparable Sr and Nd, but more radiogenic Pb isotope compositions relative to ODP Site 701[14,45,54].

Although systematic large-scale Ba isotope studies on AOC have not yet been conducted, limited published data reveal the likely influence of seawater-rock exchange through hydrothermal circulation[15]. Given that seawater in the deep ocean adjacent to AOC displays Ba isotope values of $\delta^{138/134}Ba \approx +0.2$ to +0.3‰[20,49], it is expected that these compositions form one end-member for upper AOC. The other end of the upper AOC spectrum is likely represented by the Ba isotope compositions of fresh MORBs, which exhibit Ba isotope values between $\delta^{138/134}Ba = -0.04$ and +0.15‰[19,23,24]. Therefore, the Ba isotope variation in upper AOC is theoretically expected to display $\delta^{138/134}Ba = -0.04$ to +0.30‰. This inference appears to be confirmed by reported Ba isotope values for upper AOC from Integrated Ocean Drilling Program (IODP) Site 1256 at the East Pacific Rise and Deep Sea Drilling Project Hole 442B in the Philippine Sea, which collectively show a large range of values from $\delta^{138/134}Ba = -0.01$ to +0.40‰[19,22] for samples influenced solely by typical seawater hydrothermal circulation processes. The sheeted dyke complex in IODP Site 1256 displays $\delta^{138/134}Ba$ ranging from +0.05 to +0.28‰[22], which is within the range of values observed in the upper section. Although the lower plutonic section of IODP Site 1256 shows $\delta^{138/134}Ba = -0.17$ to −0.05‰, the weighted average $\delta^{138/134}Ba$ of all AOC samples at this site is +0.17‰[22]. Given that the lower plutonic section was interpreted to be influenced by late magmatic fluids, rather than seawater-derived hydrothermal fluids[22], it is reasonable to use only the upper crustal rocks (lavas and sheeted dikes), which are predominantly affected by conventional hydrothermal alteration processes, to characterize the Ba isotope composition of AOC. These exhibit a concentration-weighted average value of $\delta^{138/134}Ba = +0.20 \pm 0.10$‰ ($n = 32$; 1 SD)[22], which is the value we use throughout this manuscript to represent AOC contributions in the SSI arc. Thus, AOC should generally be characterized by heavy Ba isotope compositions (with average $\delta^{138/134}Ba$ value of +0.20‰) compared to the upper mantle.

Discussion

No evidence for Ba isotope effects from assimilation, fractional crystallization, or post-eruption alteration

Although all samples investigated here are basalts or basaltic andesites with <59 wt.% SiO_2 (Supplementary Fig. 2), it is possible that their Ba

https://doi.org/10.1038/s41467-025-56554-x

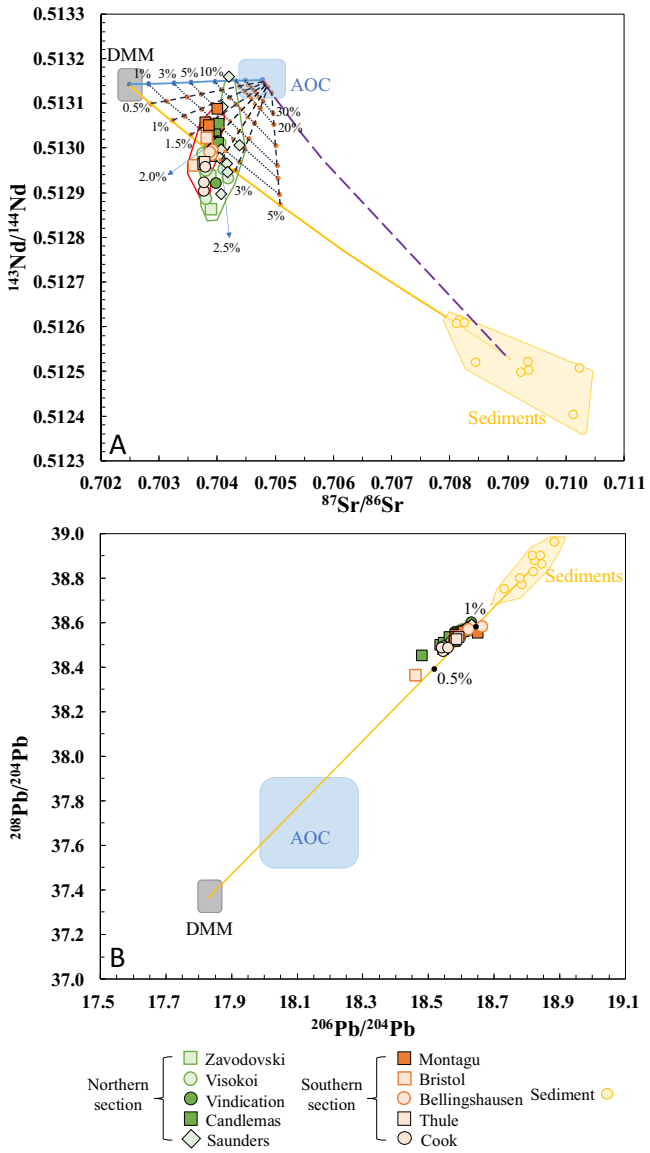

Fig. 3 | Strontium, Nd, and Pb isotope characteristics for the South Sandwich Islands (SSI) arc lavas. Plots of **A** Sr isotopes against Nd isotopes and **B** $^{206}Pb/^{204}Pb$ versus $^{208}Pb/^{204}Pb$ for the SSI arc lavas. Data for the DMM[91] and AOC[92–94] components are from the literature, and data for sediments are from this study. Mixing lines between the DMM and bulk sediments (yellow bold lines) and between the DMM and bulk AOC (blue bold line) are also shown. Numbers in mixing lines represent sediment or AOC additions by weight. Data of DMM, AOC, and sediment endmembers used for calculation in this figure are shown in Supplementary Table 6. Note that the legend colors follow that of the map in Fig. 2 and are the same for all subsequent figures with lavas from multiple locations. Source data are provided as a Source Data file.

isotope compositions have been modified by assimilation of wall rock material characterized by different isotope compositions than the original magma. These processes are expected to be most common in magmas that have experienced significant amounts of fractional crystallization (MgO < 2 wt.%). However, such magmas have been avoided in this study (Supplementary Fig. 3). No relationship between MgO (or SiO_2) and Ba/Th or Ba isotope compositions is observed for SSI arc lavas as a whole or for individual volcanoes when also considering measurement uncertainty (Supplementary Figs. 2 and 3). Notably, lavas from the adjacent islands Candlemas and Vindication display the most variable Ba isotope values and Ba/Th ratios at similar SiO_2 or MgO levels, which is distinct compared to the horizontal trends of similar Ba isotope and Ba/Th ratios with variable SiO_2 or MgO contents for all other volcanoes. These observations indicate that magmatic evolution did not cause substantial Ba isotope or Ba/Th fractionation in these samples. The variation in Ba/Th and $\delta^{138/134}Ba$ for the SSI arc lavas is more likely attributable to differences in the source regions of these magmas rather than magmatic differentiation and assimilation.

Subaerial basalt alteration has been shown to create systematically low alkali element concentrations due to leaching by meteoric water[57,58]. As Th, Rb, and Cs partition similarly in igneous processes, subaerial aqueous alteration can result in high Th/Cs and Th/Rb due to the immobile nature of Th during post-magmatic alteration processes[59]. Thus, high Th/Rb (i.e., >1) coupled with high Th/Cs (i.e., >60) might indicate subaerial alteration. Compared with data from other subaerial arcs that do not record significant alteration, we do not observe higher ratios for any samples in our study (Supplementary Fig. 4). All samples investigated here are relatively young arc lavas with ages less than 3.1 Ma[60], and fresh lava flows are unlikely to have experienced significant alteration. In addition, measured Ba isotope compositions do not correlate with Th/Rb and Th/Cs (Supplementary Fig. 5), which implies that subaerial alteration is likely limited and did not significantly affect the Ba isotope ratios of the investigated lavas. Furthermore, petrographic descriptions of the samples revealed no evidence of alteration minerals or other indicators of weathering[61].

Contribution of sediments and AOC to SSI arc lavas

Our high-precision Sr, Nd, and Pb isotope data for SSI arc lavas and proximal sediments allow an assessment of the relative importance of subducted sediments and AOC in the SSI arc lava source (Fig. 3). Previous studies have shown that the source region of the SSI arc lavas is affected by subducted sediments[60,62,63]. However, binary mixing between sediments and the depleted mantle cannot account for all the Sr and Nd isotope variations in the SSI arc. The SSI arc lavas form a trend that is almost perpendicular to the bulk sediment–mantle mixing line, which likely indicates some contributions of an AOC component with radiogenic Sr isotopes and mantle-like Nd isotopes. Indeed, the observed Pb isotope variations in the SSI lavas can be explained by simple binary mixing between the depleted mantle and sediments, without any additional AOC contributions. However, the Pb isotope mass balance calculations demonstrate that bulk sediment contributions would represent 0.5–1% by weight, which is less than the 1.5–3% by weight indicated by Sr–Nd isotope mass balance calculations (Fig. 3). This difference can be explained by the need for AOC contributions in the Pb isotope space. Since the Pb isotope compositions of AOC, DMM, and sediments fall on the same line (Fig. 3) and individual contributions are hard to disentangle, Sr isotopes may provide a more reliable estimate of bulk sediment and AOC contributions.

We also observe that SSI lavas north of the Bullard fracture zone should contain, on average, a slightly higher proportion of sediment component (2–3% by weight) than the southern section (1.5–2.5% by weight), based on Sr and Nd isotopes (Fig. 3). This observation is consistent with the age of subducted crust entering the trench from the South American plate being ~83 Ma in the north and ~27 Ma in the south[46]. Given that the oceanic crust being subducted north of ~58°S is older than that subducted south of ~58°S[52], it is expected that a thicker sedimentary layer is found outboard of the northern SSI arc compared to the southern section, as previously inferred from multichannel seismic reflection profiles, which suggested sediment thicknesses of <1 km and <0.2 km in the northern and southern SSI arc, respectively[64].

Global MORBs show variable Ba isotope compositions ranging from $\delta^{138/134}Ba = -0.04$ to +0.15‰[19,23,24]. One study found that the most depleted portion of the DMM displays the heaviest Ba isotope values of $\delta^{138/134}Ba \approx +0.08$ to +0.15‰ (with average value of $\delta^{138/134}Ba = +0.12$), with more enriched mantle components generally exhibiting lighter Ba isotope values on a global scale[19]. Two recent studies expanded the

https://doi.org/10.1038/s41467-025-56554-x

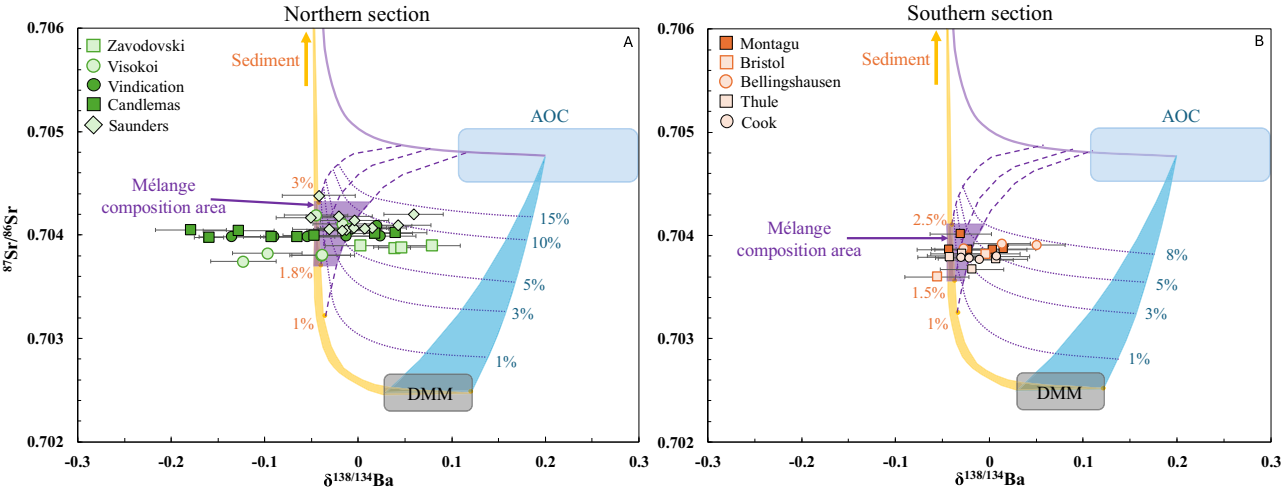

Fig. 4 | Barium and Sr isotope variations for the South Sandwich Islands (SSI) arc lavas. Mixing areas between the DMM and sediments (yellow) and between the DMM and AOC (blue) are also shown. Numbers in mixing areas represent bulk sediment or AOC additions by weight. Purple bold lines represent mixing lines between sediments and AOC. Purple dashed lines represent sediment addition to the DMM and AOC and purple dotted lines represent AOC addition to the DMM and sediment. **A** In the northern section, Ba and Sr isotope characteristics are consistent with the mélange model of slab material transport underneath the SSI arc. The purple area represents the addition of 1.8–3% by weight of sediments, and <15% of AOC, to the mantle wedge. **B** In the southern section, both the mélange model and the metasomatized mantle wedge model can account for the Ba and Sr isotope signatures for the SSI arc. The purple area represents the addition of 1.0–2.5% by weight of sediments, and <8% by weight of AOC, to the mantle wedge. Data sources for the DMM and AOC components are the same as in Fig. 1. Sediment compositions are from this study. Data of DMM, AOC, and sediment endmembers used for calculation in this figure are shown in Supplementary Table 6. Error bars associated with the $\delta^{138/134}Ba$ values represent 2 standard deviations (SD) of sample reproducibility. Source data are provided as a Source Data file.

MORB dataset and argued that the most common Ba isotope composition of the DMM end-member should be $\delta^{138/134}Ba = +0.03$ to +0.05‰[23,24]. In order to accommodate all views of the Ba isotope composition of DMM, we here use a range of $\delta^{138/134}Ba$ values from +0.03 to +0.12‰ rather than a single point ($\delta^{138/134}Ba = +0.03$, +0.05 or +0.12‰) to represent Ba isotope compositions of DMM (see Supplementary Information for discussion of the DMM value). SSI arc lavas have Ba isotope values ranging from −0.18 to +0.08‰ (Fig. 2), which is significantly lighter than DMM. Given that magmatic processes such as fractional crystallization and assimilation cannot account for the observed Ba isotope variations, it is reasonable to infer that components from the subducting slab (e.g., marine sediments and/or AOC) with lighter Ba isotope compositions than the mantle are the main cause of the light Ba isotope characteristics in the SSI arc lavas. Because AOC displays Ba concentrations about two orders of magnitude lower than those of marine sediments[14,65], and much heavier Ba isotope characteristics than the DMM[19,22], we reason that AOC cannot account for the light Ba isotope characteristics observed in the SSI arc lavas. Based on these arguments, Ba isotope compositions in most SSI arc lavas should result from inheriting the Ba isotope characteristics of subducting pelagic sediments outboard of the SSI trench, consistent with the fact that all SSI lavas exhibit lighter Ba isotope compositions than the DMM (Fig. 2).

Sources and processes of fluid and melt release underneath the SSI arc

The primary difference between the two end-member models of slab-to-mantle wedge material transport lies in the sequence of events that lead to the combination of various components to ultimately form arc magmas[4]. Our stable Ba isotope data, coupled with radiogenic Sr, Nd, and Pb isotope data, demonstrate that, although AOC does influence the SSI arc, subducted sediment is the dominant Ba input to the source of the SSI arc lavas. This is most evident in the northern section where the subducted sediment thickness is greatest. However, arc lavas throughout the northern part of the SSI reveal Ba isotope values both lighter (Candlemas and Vindication islands; as light as $\delta^{138/134}Ba = -0.18$‰) and heavier (Zavodovski and Saunders; as heavy as $\delta^{138/134}Ba = +0.08$‰) than sedimentary inputs ($\delta^{138/134}Ba = -0.10$ to 0.00‰). This suggests that some Ba isotope fractionation occurs during the transport of subducted sediments within the subducting slab, as has been inferred in other arcs[15]. Our Ba isotope data, used in combination with radiogenic isotope ratios, help determine whether Ba isotope fractionation occurred during sediment melting and/or AOC dehydration before slab components mixed with the mantle wedge (metasomatized mantle wedge model), or whether sediments, AOC, and mantle components mixed together at the slab–mantle interface before Ba isotope fractionation occurred during mélange melting and/or dehydration (mélange model). As described in the introduction, an effective means of discriminating the two models is by using plots of $^{87}Sr/^{86}Sr$ versus $\delta^{138/134}Ba$ (Fig. 1).

In the SSI arc, especially in the northern section, arc lavas exhibit limited Sr isotope variation, whereas Ba isotope compositions are highly variable, producing an almost horizontal trend in a Sr–Ba isotope plot (Fig. 4). These characteristics are difficult to account for by mixing slab-derived fluids and sediment melts with a mantle source, as these should produce sub-vertical trends (Fig. 1A). In contrast, the horizontal data array is readily explained by dehydration and/or melting of a mélange underneath the SSI arc that generates Ba isotope fractionation. The Ba isotope variability of the assumed mélange compositions (purple field in Fig. 4) reflects some of the inherent heterogeneity of natural mélanges[28,41,42,66], even though they do not account for the entire Ba isotope range of the SSI lavas. In contrast, the mélange has a limited range of Sr–Nd isotope compositions, which results from the average proportion of the subducted sediment component only varying by a factor of three for the entire arc (1–3%; Fig. 3). In theory, mélange compositions can straddle a large field between sediments, AOC, and DMM (Fig. 4), but the Sr–Nd isotope variations in northern SSI lavas are relatively small and provide some constraints on possible mélange compositions. The source under the northern section of the SSI arc may comprise 1.8–3% by weight of sediments, and <15% of AOC (Figs. 3 and 4). In the southern part of SSI arc, bulk sediment and AOC contributions to the source could account for 1.0 – 2.5% and <8% by weight, respectively (Figs. 3 and 4), consistent with thicker sediment cover on the subducting slab in the north.

https://doi.org/10.1038/s41467-025-56554-x

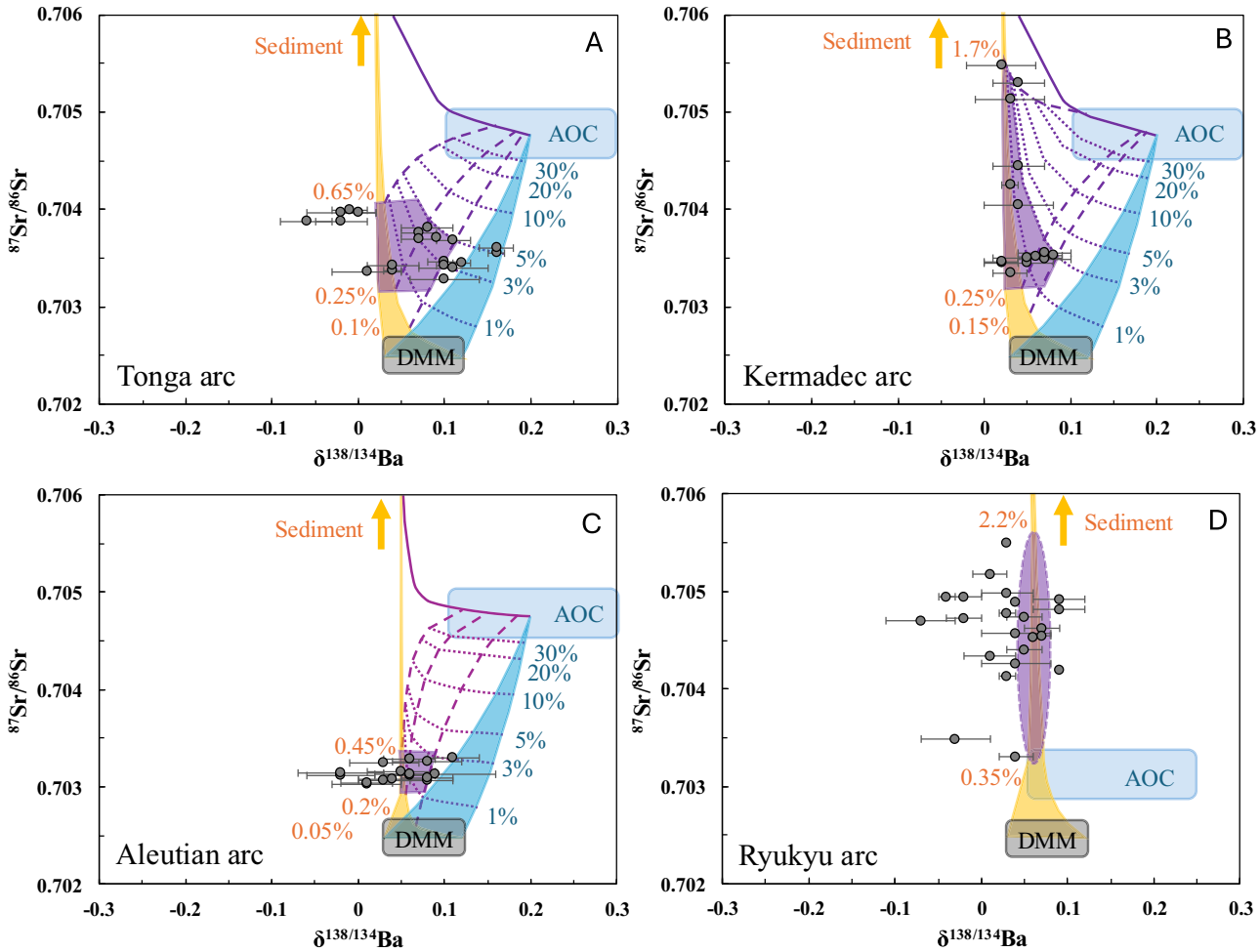

Fig. 5 | Barium and Sr isotope variations for Tonga, Kermadec, Aleutian, and Ryukyu arcs. Mixing areas between the DMM and sediments (yellow) and between the DMM and AOC (blue) are also shown. Numbers in mixing areas represent bulk sediment or AOC additions by weight. Purple bold lines represent mixing lines between sediments and AOC. Purple dashed lines represent sediment addition to the DMM and AOC and purple dotted lines represent AOC addition to the DMM and sediment. **A** The purple area represents addition of 0.1–0.65% by weight of sediments, and <5% by weight of AOC, to the mantle wedge. **B** The purple area represents addition of 0.15–1.7% by weight of sediments, and <3% by weight of AOC, to the mantle wedge. **C** The purple area represents addition of 0.05–0.45% by weight of sediments, and <3% by weight of AOC, to the mantle wedge. **D** The purple area represents addition of 0.35–2.2% by weight of sediments to the mantle wedge. Data sources for the DMM and AOC (**A**–**C**) components are the same as in Fig. 1. Arc lava and sediment compositions in (**A**, **B**)[16], (**C**)[15,96], and (**D**)[15,67], as well as AOC data in (**D**)[15,67], are from previous studies. Data of DMM, AOC, and sediment endmembers used for calculation in this figure are shown in Supplementary Table 7. Error bars associated with the $\delta^{138/134}$Ba values represent 2 standard deviations (SD) of sample reproducibility.

Although the northern section of the SSI arc displays a horizontal trend in Ba–Sr isotope space that can only be attributed to mélange formation, the southern section of the arc could either be consistent with more weakly developed mélange formation or with the metasomatized mantle wedge model. Melting or dehydration of the weakly developed mélange underneath the southern section of the arc did not result in Ba isotope fractionation. Otherwise, Ba and Sr isotope variations in the southern section reflect mixing between the DMM and sediment-dominant melts. The current data do not permit distinguishing between the two models. When considering Ba–Sr isotope data from other arcs, it is also apparent that similar trends to the northern and southern sections of the SSI can be observed. Data from the Tonga and Aleutian arcs reveal similar trends to the northern SSI (Fig. 5), that appear most consistent with mélange dehydration and/or melting. However, both the Ryukyu and Kermadec arcs show Sr–Ba isotope variability that could be consistent with either melt generation within mélanges[67], or processes related to mantle metasomatism[16], or a combination of both.

In the following section, we investigate how mineral breakdown reactions associated with dehydration and melting within a mélange could have affected the Ba isotope and trace element signatures of the northern section of the SSI arc, and how similar mélange processes or melt generation from metasomatized mantle wedge could have affected the Ba isotope and trace element signatures of the southern section of the SSI arc.

Barium isotope fractionation during mélange dehydration and melting underneath the northern SSI arc

We employ the Ba isotope characteristics of the northern section of the SSI arc, and their relationship with other tracers of fluid and melt release, to investigate the processes that may cause Ba isotope fractionation during mélange dehydration and melting. Barium isotope fractionation during subduction-related metamorphism has been observed in eclogites and associated veins, which reveal that heavy Ba isotopes are preferentially extracted by aqueous fluids during partial decomposition of the minerals lawsonite and phengite, whereas light Ba isotopes are preferentially enriched in residual minerals (e.g., phengite) at depths approximating the source zones of arc magmas[36,37]. Some mélanges may start melting at subarc magma generation depths (~2.5 GPa) within a low-temperature range of

700–900 °C[29], that would favor the Ba isotope fractionations observed in exhumed metamorphic rocks from slab tops. In combination, mélange melting experiments and metamorphic Ba isotope data allow for Ba isotope fractionation during mélange melting, both at the slab-top as well as during diapirism depending on where melting starts due to the arc thermal structure[29]. Arc lavas from different volcanoes likely represent different degrees of melting and have undergone different magma processes (e.g., fractional crystallization) that can strongly affect the absolute concentration of a trace element like Ba. Instead, we prefer to use trace element ratios in which two elements show similar compatibilities during partial melting and fractional crystallization, rather than absolute trace element concentrations for further discussion.

Candlemas and Vindication lavas display lighter $\delta^{138/134}$Ba than any of the components that make up the mélange, which could indicate the occurrence of Ba isotope fractionations during the generation of the magmas. The residual phengite is the host of light Ba isotopes during dehydration of hydrous minerals in the subducted slab[36]. We speculate that the Ba isotope fractionations in the Candlemas and Vindication lavas could result from complete breakdown of residual phengite with light Ba isotope compositions in the source after early pulses of partial dehydration of phengite in the slab liberated the heavy Ba isotopes[36,37]. Candlemas and Vindication volcanoes are also characterized by high and variable Ba/Th, high Sr/Nd, and low U/Ba (Fig. 6), consistent with the final breakdown of Ba-bearing minerals like phengite[6]. Although Ba is highly fluid-mobile[2,3,8], phengite is the primary mineral that can accommodate Ba in the subducted slab at arc magma generation depths[9,68] but is not enriched in U and, thus, phengite breakdown would produce fluids with low U/Ba[9,69,70]. Lavas influenced by complete breakdown and melting of residual phengite with light $\delta^{138/134}$Ba in a mélange, as hypothesized for Candlemas and Vindication volcanoes, thus should contain higher Ba concentrations than those produced with phengite in the mélange residue[37]. Despite strong arguments for phengite dehydration, the exact nature of the dehydrating mineral does not change the main results of our study.

Zavodovski and Saunders volcanoes display heavier $\delta^{138/134}$Ba signatures (−0.05 to +0.08‰), indicating that the source of these volcanoes is affected by dehydration fluids as hydrous fluids prefer to take up heavy Ba isotopes during partial decomposition of lawsonite and phengite[36,37]. These volcanoes are also characterized by lower Ba/Th and Sr/Nd and higher U/Ba than Candlemas and Vindication volcanoes. Lawsonite is a main host for light rare earth elements (e.g., Nd), Sr, U, and Th, but does not contain significant quantities of alkali metals[71–73]. Fluids derived from lawsonite-out reactions should therefore be characterized by relatively high U/Ba and low Ba/Th, which is consistent with the trace element ratios in Zavodovski and Saunders volcanoes. In addition, arc lavas generated from breakdown of lawsonite with residual phengite in the mélange, as hypothesized for Zavodovski and Saunders volcanoes, should also display lower Sr/Nd than lavas that record the complete breakdown of phengite[6]. Visokoi volcano is more challenging to interpret as it displays light $\delta^{138/134}$Ba (−0.12 to −0.01‰) similar to Candlemas and Vindication volcanoes that record phengite breakdown, but shares the trace element characteristics of Zavodovski and Saunders volcanoes (low Ba/Th, low Sr/Nd, high U/Ba), interpreted to record lawsonite breakdown with residual phengite. It may represent a transition between these two stages, where incipient breakdown of residual phengite with light $\delta^{138/134}$Ba is accompanied by near-complete breakdown of lawsonite. Accessory phases such as monazite, allanite, and zircon may also affect the mobilities of U, Th, Sr, and Nd[10,12,30,74]; however, to a first order, lawsonite and phengite stabilities are broadly consistent with the observed trace element variations.

It is worth noting that the volcanoes associated with lawsonite breakdown and residual phengite (Zavodovski and Saunders) present rear-arc magmatism and associated seamount chains, while the volcanoes showing evidence of phengite breakdown (Candlemas and Vindication) do not (Fig. 2). The seamount chains were hypothesized to be tectonically controlled by parallel NE–SW fractures of the Sandwich plate[75]. Although we do not have compositional data for the rear-arc, they structurally resemble the rear-arc volcanoes of the Izu arc in the Western Pacific[76]. The presence of fractures likely enhanced melt focusing mechanisms around the volcanoes, but while lawsonite and ultimately phengite were still available in the source of Zavodovski and Saunders volcanoes, Vindication and Candlemas volcanoes record a more advanced stage of phengite breakdown, which may indicate reduced hydrous mineral abundances and source fertility, thus an inability to produce noticeable rear-arc magmatism.

Barium isotope signatures of AOC dehydration and sediment melting underneath the southern SSI arc

Bristol, Bellingshausen, Thule, and Cook lavas are associated with relatively high U/Ba and low Ba/Th (Fig. 6). These patterns are similar to Zavodovski and Saunders volcanoes, but with a much narrower range of Ba isotope compositions (Fig. 6). In these volcanoes, trace element fractionations and Ba–Sr isotope characteristics would most simply be explained by fluids derived from lawsonite breakdown with residual phengite in the AOC, mixed with sediment melts, consistent with a metasomatized mantle wedge model (Fig. 1). A mélange source is not required, though it is not precluded either. These lavas display Ba isotope compositions of $\delta^{138/134}$Ba = −0.06 to +0.05‰ (Fig. 6), which could indicate Ba isotope fractionation during partial decomposition of lawsonite or phengite or both within a mélange, or reflect sediment melting, or a combination of both (Figs. 4 and 6). The sediment component underneath the southern section is less voluminous than beneath the northern section, as revealed by radiogenic isotopes (Figs. 3 and 4) and multichannel seismic reflection data[64]. Montagu volcano exhibits indistinguishable Ba isotope compositions compared to Bristol, Bellingshausen, Thule, and Cook volcanoes, but displays high Ba/Th, the highest Sr/Nd of the entire chain, and low U/Ba (Fig. 6), which could indicate significant fluid release from deep-seated phengite in AOC or mélange. Residual phengite with light $\delta^{138/134}$Ba may be carried within the AOC or mélange into the deep mantle. Montagu sits at the boundary between the old subducting plate to the north and the young subducting plate to the south and may have experienced a higher influx of fluids due to its particular location. The southern half of the subducted plate beneath the SSI arc is considerably younger, and likely warmer and more buoyant, compared to the old and dense northern half[46,52]. It can be speculated that the thin sediment cover in the southern section could have melted to a large degree before a thick, relatively cold mélange had time to form.

In conclusion, we combined Ba isotope systematics, radiogenic Sr, Nd, and Pb isotopes, and trace element ratios in SSI lavas and sediments to discern mechanisms of subducted material transfer in the SSI subduction zone. Our results reveal that the northern section of the arc primarily records mélange dehydration and melting. Mélange formation in this region is favored by the relatively thick sediment cover and colder subducting oceanic plate. Progressive dehydration of different hydrous minerals in the mélange, comprising mantle wedge, subducted sediments, and AOC, accounts for the variability in trace element and Ba isotope compositions. Although the presence of a mélange cannot be precluded in the southern section, volcanoes in the southern SSI arc are most simply consistent with a contrasting metasomatized mantle wedge model. In this model, AOC dehydrates and sediments melt early on due to the thinner sediment cover and warmer slab-top conditions. The unique Ba isotope signatures of subducting sediments at these latitudes make the SSI arc a truly exceptional setting to evaluate the utility of Ba isotopes in studying subduction processes. Our findings show that slab material transport mechanisms vary between different arcs and also within a single system, as exemplified by the SSI arc.

https://doi.org/10.1038/s41467-025-56554-x

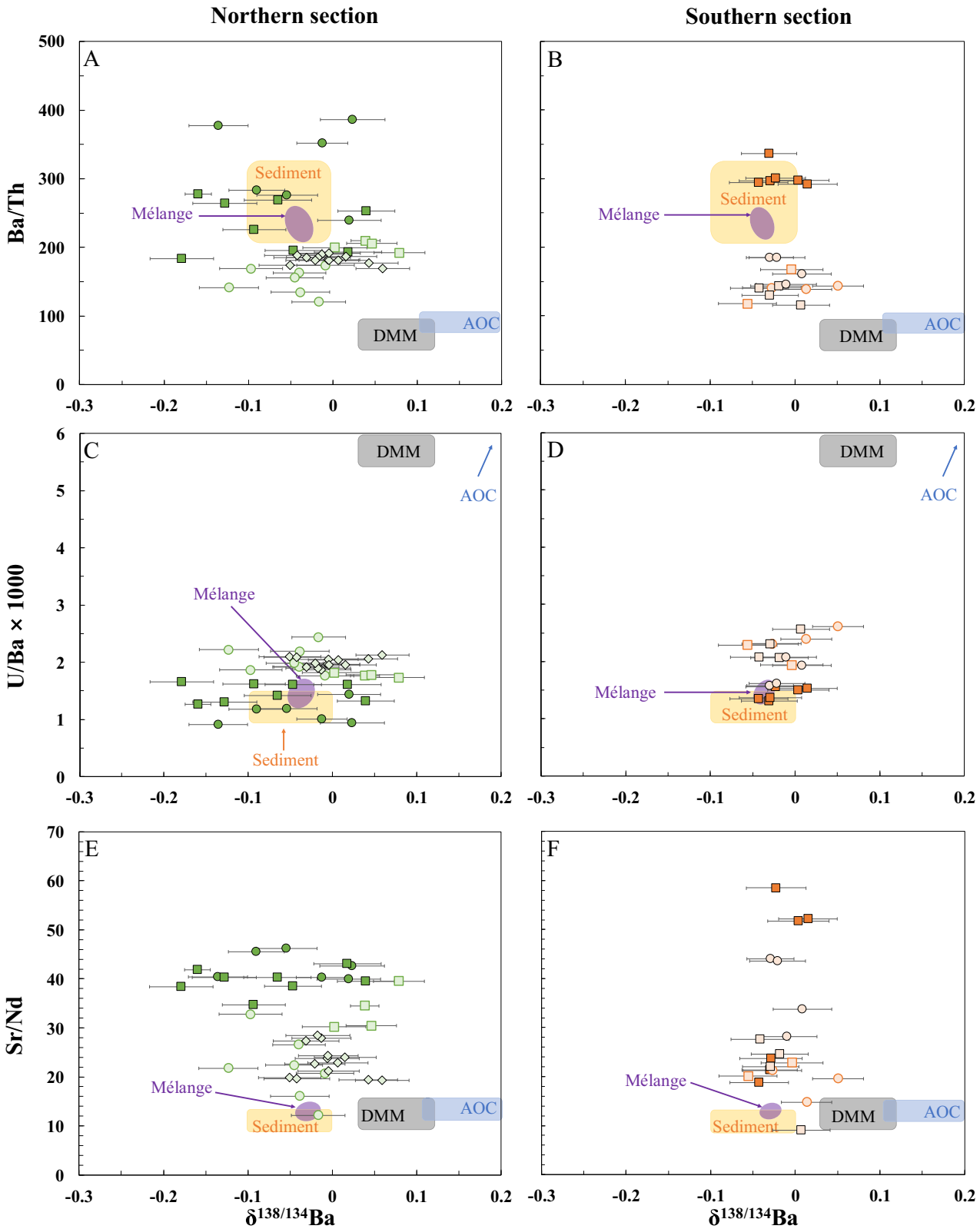

Fig. 6 | Trace element and Ba isotope compositions in the South Sandwich Islands (SSI) arc lavas indicate breakdown of different minerals at subarc depths. Barium isotope compositions plotted versus Ba/Th, U/Ba, and Sr/Nd for northern (**A**, **C**, **E**) and southern (**B**, **D**, **F**) parts of SSI arc lavas. Data sources for the DMM, AOC, and sediment components are the same as in Fig. 4. Also shown are source compositions (purple areas) calculated by similar contributions of sediment and AOC to the DMM as in Fig. 4 underneath the northern and southern parts of the SSI arc. Error bars associated with the $\delta^{138/134}$Ba values represent 2 standard deviations (SD) of sample reproducibility. Source data are provided as a Source Data file.

Methods

We have analyzed the Ba isotope compositions of 63 arc magmas from the SSI arc, supplemented by analysis of 9 sediment samples from sediment cores outboard of the SSI trench. Samples were dissolved in 1:1 mixtures of concentrated HF and HNO_3 on a hotplate overnight followed by evaporation and repeated refluxing in concentrated HNO_3 to remove fluorides. Sample aliquots containing ~50 ng of Ba were isolated from each sample and spiked with an appropriate quantity of ^{135}Ba–^{136}Ba double spike[77] prior to ion-exchange separation (Supplementary Information). The ion-exchange separation was conducted using AG 50W-X8 cation exchange resin (200–400 mesh). Spiked samples were dissolved in 250 µL of 2 M HCl and passed through 500 µL of resin in the NIRVANA Laboratories at the Woods Hole Oceanographic Institution (WHOI)[49]. The majority of the sample matrix, including major elements, was eluted with 2 M HCl and Ba was subsequently eluted with 2 M HNO_3[49]. This protocol is based on established procedures[78,79], noting that Ba and other Group II elements show no absorption to AG 50W-X8 resin in HNO_3. In contrast, rare earth elements, such as isobaric La and Ce, are strongly retained. Following the elution of Ba, samples were evaporated to dryness, reconstituted in 2 M HCl and the ion-exchange procedure was repeated using fresh resin.

Barium isotope measurements were performed using a Thermo-Finnigan *Neptune* multi-collector inductively coupled plasma mass spectrometer (MC-ICP-MS) situated in the WHOI Plasma Facility. Samples and standards were aspirated at ≈140 µL min^{-1} using a PFA nebulizer and desolvated using an Aridus II. Analyses comprised 30 s of baseline monitoring (in 1 s integrations), followed by 30 × 4.2 s integrations of sample solution, and a 90 s washout between samples. Instrumental and sample mass fractionation was calculated by solving for Ba isotope compositions relative to the double spike using a MATLAB-based code for spike-sample deconvolution. Each sample was typically analyzed four times, and final Ba isotope compositions are reported as the weighted mean of these four measurements relative to similarly spiked aliquots of NIST SRM 3104a. The precision of our Ba isotope analyses is reported as either the long-term ±2 SD of sample unknowns (±0.03 ‰), or the ±2 SE of the four replicate measurements of the samples, whichever is larger. The accuracy of our Ba isotope data was assessed by passing four international reference materials, BHVO-1 and G-2 (USGS) and JA-2 and JCp-1 (GSJ), through our processing procedures alongside sample unknowns. Our results for these standards fall within the uncertainty of previously reported compositions[49,80,81] and are reported in full in Supplementary Table 8.

Strontium, Nd, and Pb were separated from the matrix of samples using previously published ion-exchange chromatographic methods[82–84]. Their isotope compositions for SSI arc lavas and sediments were determined using the Neptune MC-ICP-MS, located in the WHOI Plasma Facility, following published methods[82–84]. All results were corrected against the Sr reference material NIST SRM 987 ($^{87}Sr/^{86}Sr = 0.710240$)[85], JNdi-1 value of $^{143}Nd/^{144}Nd = 0.512104$[86,87], and NIST SRM 981 Pb reference material ($^{206}Pb/^{204}Pb = 16.9356$, $^{207}Pb/^{204}Pb = 15.4891$, $^{208}Pb/^{204}Pb = 36.7006$)[88]. The well-characterized USGS reference material BHVO-1 was measured as unknown. Its results for Sr, Nd, and Pb were $^{87}Sr/^{86}Sr = 0.703466$, $^{143}Nd/^{144}Nd = 0.512980$, $^{206}Pb/^{204}Pb = 18.694$, $^{207}Pb/^{204}Pb = 15.574$, and $^{208}Pb/^{204}Pb = 38.361$, which are within error of published values[89].

Trace element concentrations were determined for all samples using an ICAP-Q ICP-MS at WHOI. Concentrations were calculated via reference to ion beam intensities obtained from a four-point calibration curve constructed by analyzing serial dilutions of a gravimetrically prepared four rock reference materials (AGV-1, BCR-1, BHVO-1, and BIR-1) with recommended concentrations[90]. Each sample was doped with indium (In) before measurement, and drift was monitored and corrected via normalization to In intensities. The precision and accuracy of these analyses are between 5 and 10% based on the measurement of additional dissolutions of the same USGS rock reference materials as unknowns during the same analysis runs (Supplementary Table 9).

Data availability

All data needed to evaluate the conclusion in the paper are present in the paper and the Supplementary Materials. Source data generated in this study have been deposited in the Zenodo database (https://doi.org/10.5281/zenodo.14674281). Source data are provided with this paper.

References

1. Ishikawa, T. & Nakamura, E. Origin of the slab component in arc lavas from across-arc variation of B and Pb isotopes. *Nature* **370**, 205–208 (1994).
2. Elliott, T., Plank, T., Zindler, A., White, W. & Bourdon, B. Element transport from slab to volcanic front at the Mariana arc. *J. Geophys. Res. Solid Earth* **102**, 14991–15019 (1997).
3. Kessel, R., Schmidt, M. W., Ulmer, P. & Pettke, T. Trace element signature of subduction-zone fluids, melts and supercritical liquids at 120–180 km depth. *Nature* **437**, 724–727 (2005).
4. Nielsen, S. G. & Marschall, H. R. Geochemical evidence for mélange melting in global arcs. *Sci. Adv.* **3**, e1602402 (2017).
5. Spandler, C. & Pirard, C. Element recycling from subducting slabs to arc crust: a review. *Lithos* **170-171**, 208–223 (2013).
6. Shu, Y. et al. Sources of dehydration fluids underneath the Kamchatka arc. *Nat. Commun.* **13**, 4467 (2022).
7. Behn, M. D., Kelemen, P. B., Hirth, G., Hacker, B. R. & Massonne, H.-J. Diapirs as the source of the sediment signature in arc lavas. *Nat. Geosci.* **4**, 641–646 (2011).
8. Elliott, T. Tracers of the slab. *Geophys. Monogr. Am. Geophys. Union* **138**, 23–46 (2003).
9. Bebout, G. E. Metamorphic chemical geodynamics of subduction zones. *Earth Planet Sci. Lett.* **260**, 373–393 (2007).
10. Carter, L. B., Skora, S., Blundy, J. D., De Hoog, J. C. M. & Elliott, T. An experimental study of trace element fluxes from subducted oceanic crust. *J. Pet.* **56**, 1585–1606 (2015).
11. Skora, S. & Blundy, J. High-pressure hydrous phase relations of radiolarian clay and implications for the involvement of subducted sediment in arc magmatism. *J. Pet.* **51**, 2211–2243 (2010).
12. Klimm, K., Blundy, J. D. & Green, T. H. Trace element partitioning and accessory phase saturation during H_2O-saturated melting of basalt with implications for subduction zone chemical fluxes. *J. Pet.* **49**, 523–553 (2008).
13. Keppler, H. Constraints from partitioning experiments on the composition of subduction-zone fluids. *Nature* **380**, 237–240 (1996).
14. Plank, T. & Langmuir, C. H. The chemical composition of subducting sediment and its consequences for the crust and mantle. *Chem. Geol.* **145**, 325–394 (1998).
15. Nielsen, S. G. et al. Barium isotope systematics of subduction zones. *Geochim. Cosmochim. Acta* **275**, 1–18 (2020).
16. Wu, F., Turner, S. & Schaefer, B. F. Mélange versus fluid and melt enrichment of subarc mantle: a novel test using barium isotopes in the Tonga-Kermadec arc. *Geology* **48**, 1053–1057 (2020).
17. Hao, L.-L. et al. Mg-Ba-Sr-Nd isotopic evidence for a mélange origin of early Paleozoic arc magmatism. *Earth Planet Sci. Lett.* **577**, 117263 (2022).
18. Yu, H.-M. et al. Barium isotope evidence of a fluid-metasomatized mantle component in the source of Azores OIB. *Chem. Geol.* **610**, 121097 (2022).
19. Nielsen, S. G. et al. Barium isotope evidence for pervasive sediment recycling in the upper mantle. *Sci. Adv.* **4**, eaas8675 (2018).
20. Bridgestock, L. et al. Controls on the barium isotope compositions of marine sediments. *Earth Planet Sci. Lett.* **481**, 101–110 (2018).

21. Bridgestock, L., Hsieh, Y.-T., Porcelli, D. & Henderson, G. M. Increased export production during recovery from the Paleocene–Eocene thermal maximum constrained by sedimentary Ba isotopes. *Earth Planet Sci. Lett.* **510**, 53–63 (2019).
22. Nan, X. et al. Barium isotope compositions of altered oceanic crust from the IODP Site 1256 at the East Pacific rise. *Chem. Geol.* **641**, 121778 (2023).
23. Nan, X., Yu, H., Kang, J. & Huang, F. Re-visiting barium isotope compositions of mid-ocean ridge basalts and the implications. *JUSTC* **52**, 1 (2022).
24. Wu, F. et al. Barium isotope composition of depleted MORB mantle constrained by basalts from the South Mid-Atlantic Ridge (5–11°S) with implication for recycled components in the convecting upper mantle. *Geochim. Cosmochim. Acta* **340**, 85–98 (2023).
25. Class, C., Miller, D. M., Goldstein, S. L. & Langmuir, C. H. Distinguishing melt and fluid subduction components in Umnak Volcanics, Aleutian Arc. *Geochem. Geophys. Geosyst.* **1**, 1004 (2000).
26. Kelemen, P., Hanghøj, K. & Greene, A. One view of the geochemistry of subduction-related magmatic arcs, with an emphasis on primitive andesite and lower crust. *Treatise Geochem.* **3**, 659 (2003).
27. Marschall, H. R. & Schumacher, J. C. Arc magmas sourced from mélange diapirs in subduction zones. *Nat. Geosci.* **5**, 862–867 (2012).
28. Bebout, G. E. & Penniston-Dorland, S. C. Fluid and mass transfer at subduction interfaces—the field metamorphic record. *Lithos* **240-243**, 228–258 (2016).
29. Codillo, E. A. et al. The ascent of subduction zone mélanges: experimental constraints on mélange rock densities and solidus temperatures. *Earth Planet Sci. Lett.* **621**, 118398 (2023).
30. Hermann, J. & Rubatto, D. Accessory phase control on the trace element signature of sediment melts in subduction zones. *Chem. Geol.* **265**, 512–526 (2009).
31. Hermann, J. & Spandler, C. J. Sediment melts at sub-arc depths: an experimental study. *J. Pet.* **49**, 717–740 (2008).
32. Li, H., Hermann, J. & Zhang, L. Melting of subducted slab dictates trace element recycling in global arcs. *Sci. Adv.* **8**, eabh2166 (2022).
33. Kodolányi, J., Pettke, T., Spandler, C., Kamber, B. S. & Gméling, K. Geochemistry of ocean floor and fore-arc serpentinites: constraints on the ultramafic input to subduction zones. *J. Pet.* **53**, 235–270 (2011).
34. Debret, B. et al. Trace element behavior during serpentinization/deserpentinization of an eclogitized oceanic lithosphere: A LA-ICPMS study of the Lanzo ultramafic massif (Western Alps). *Chem. Geol.* **357**, 117–133 (2013).
35. Deschamps, F. et al. Behavior of fluid-mobile elements in serpentines from abyssal to subduction environments: Examples from Cuba and Dominican Republic. *Chem. Geol.* **312-313**, 93–117 (2012).
36. Gu, X.-F., Guo, S., Yu, H., Xu, J. & Huang, F. Behavior of barium isotopes during high-pressure metamorphism and fluid evolution. *Earth Planet Sci. Lett.* **575**, 117176 (2021).
37. Xu, J. et al. Barium isotope fractionation during slab dehydration: records from an eclogite-quartz vein system in Dabie orogen. *Geochim Cosmochim. Acta* **343**, 272–285 (2023).
38. Crockford, P. W. et al. Barium-isotopic constraints on the origin of post-Marinoan barites. *Earth Planet Sci. Lett.* **519**, 234–244 (2019).
39. Cruz-Uribe, A. M., Marschall, H. R., Gaetani, G. A. & Le Roux, V. Generation of alkaline magmas in subduction zones by partial melting of mélange diapirs—an experimental study. *Geology* **46**, 343–346 (2018).
40. Codillo, E. A., Le Roux, V. & Marschall, H. R. Arc-like magmas generated by melange-peridotite interaction in the mantle wedge. *Nat. Commun.* **9**, 2864 (2018).
41. Spandler, C., Hermann, J., Faure, K., Mavrogenes, J. A. & Arculus, R. J. The importance of talc and chlorite "hybrid" rocks for volatile recycling through subduction zones; evidence from the high-pressure subduction mélange of New Caledonia. *Contrib. Miner. Pet.* **155**, 181–198 (2008).
42. Bebout, G. E. & Barton, M. D. Tectonic and metasomatic mixing in a high-T, subduction-zone mélange—insights into the geochemical evolution of the slab–mantle interface. *Chem. Geol.* **187**, 79–106 (2002).
43. Workman, R. K. & Hart, S. R. Major and trace element composition of the depleted MORB mantle (DMM). *Earth Planet Sci. Lett.* **231**, 53–72 (2005).
44. Leat, P. T., Larter, R. D. & Millar, I. L. Silicic magmas of Protector Shoal, South Sandwich arc: Indicators of generation of primitive continental crust in an island arc. *Geol. Mag.* **144**, 179–190 (2006).
45. Liu, E. J. et al. Volcanic activity and gas emissions along the South Sandwich arc. *Bull. Volcano.* **83**, 1–23 (2021).
46. Barker, P. F. Tectonic framework of the east Scotia Sea. in *Backarc Basins* 281–314 (Springer US, 1995).
47. Vanneste, L. E. & Larter, R. D. Sediment subduction, subduction erosion, and strain regime in the northern South Sandwich forearc. *J. Geophys. Res. Solid Earth* **107**, EPM 5-1–EPM 5-24 (2002).
48. Jacquet, S. et al. Mesopelagic organic carbon remineralization in the Kerguelen Plateau region tracked by biogenic particulate Ba. *Deep Sea Res Part II Top. Stud. Oceanogr.* **55**, 868–879 (2008).
49. Horner, T. J., Kinsley, C. W. & Nielsen, S. G. Barium-isotopic fractionation in seawater mediated by barite cycling and oceanic circulation. *Earth Planet Sci. Lett.* **430**, 511–522 (2015).
50. Horner, T. J. et al. Pelagic barite precipitation at micromolar ambient sulfate. *Nat. Commun.* **8**, 1342 (2017).
51. Hsieh, Y.-T. & Henderson, G. M. Barium stable isotopes in the global ocean: tracer of Ba inputs and utilization. *Earth Planet Sci. Lett.* **473**, 269–278 (2017).
52. Brett, C. Seismicity of the South Sandwich Islands region. *Geophys. J. Int.* **51**, 453–464 (1977).
53. Barker, P. F. & Lawver, L. A. South American-Antarctic plate motion over the past 50 Myr, and the evolution of the South American-Antarctic Ridge. *Geophys. J. Int.* **94**, 377–386 (1988).
54. Tonarini, S., Leeman, W. P. & Leat, P. T. Subduction erosion of forearc mantle wedge implicated in the genesis of the South Sandwich Island (SSI) arc: evidence from boron isotope systematics. *Earth Planet Sci. Lett.* **301**, 275–284 (2011).
55. Horner, T. J. & Crockford, P. W. *Barium Isotopes: Drivers, Dependencies, and Distributions Through Space and Time* (Cambridge University Press, 2021).
56. Mete, Ö. et al. Barium in seawater: dissolved distribution, relationship to silicon, and barite saturation state determined using machine learning. *Earth Syst. Sci. Data* **15**, 4023–4045 (2023).
57. Feigenson, M. D., Hofmann, A. W. & Spera, F. J. Case studies on the origin of basalt. *Contrib. Miner. Pet.* **84**, 390–405 (1983).
58. Schiano, P., Dupré, B. & Lewin, E. Application of element concentration variability to the study of basalt alteration (Fangataufa atoll, French Polynesia). *Chem. Geol.* **104**, 99–124 (1993).
59. Hecht, L., Thuro, K., Plinninger, R. & Cuney, M. Mineralogical and geochemical characteristics of hydrothermal alteration and episyenitization in the Königshain granites, northern Bohemian Massif, Germany. *Int. J. Earth Sci.* **88**, 236–252 (1999).
60. Leat, P., Smellie, J., Millar, I. & Larter, R. Magmatism in the South Sandwich arc. *Geol. Soc. Spec. Publ.* **219**, 285–313 (2003).
61. Baker, P. E. *The South Sandwich Islands: III. Petrology of the Volcanic Rocks* (British Antarctic Survey, 1978).
62. Leat, P. T. et al. Magma genesis and mantle flow at a subducting slab edge: the South Sandwich arc-basin system. *Earth Planet Sci. Lett.* **227**, 17–35 (2004).
63. Barry, T. L., Pearce, J. A., Leat, P. T., Millar, I. L. & le Roex, A. P. Hf isotope evidence for selective mobility of high-field-strength elements in a subduction setting: South Sandwich Islands. *Earth Planet Sci. Lett.* **252**, 223–244 (2006).

64. Larter, R. D., Vanneste, L. E., Morris, P. & Smythe, D. K. Structure and tectonic evolution of the South Sandwich arc. *Geol. Soc. Spec. Publ.* **219**, 255–284 (2003).
65. Gao, Y., Huang, J. & Casey, J. F. Data report: trace element geochemistry of oceanic crust formed at superfast-spreading ridge, Hole 1256D. *Proc. IODP* **309**, 312 (2009).
66. King, R., Bebout, G., Moriguti, T. & Nakamura, E. Elemental mixing systematics and Sr–Nd isotope geochemistry of mélange formation: obstacles to identification of fluid sources to arc volcanics. *Earth Planet Sci. Lett.* **246**, 288–304 (2006).
67. Shu, Y. et al. Tracing subducted sediment inputs to the Ryukyu arc-Okinawa Trough system: evidence from thallium isotopes. *Geochim. Cosmochim. Acta* **217**, 462–491 (2017).
68. Zack, T., Rivers, T. & Foley, S. Cs–Rb–Ba systematics in phengite and amphibole: an assessment of fluid mobility at 2.0 GPa in eclogites from Trescolmen, Central Alps. *Contrib. Miner. Pet.* **140**, 651–669 (2001).
69. Guo, S. et al. Fluid–rock interaction and element mobilization in UHP metabasalt: constraints from an omphacite–epidote vein and host eclogites in the Dabie orogen. *Lithos* **136-139**, 145–167 (2012).
70. Guo, S. et al. Formation of multiple high-pressure veins in ultrahigh-pressure eclogite (Hualiangting, Dabie terrane, China): fluid source, element transfer, and closed-system metamorphic veining. *Chem. Geol.* **417**, 238–260 (2015).
71. Martin, L. A. J. et al. Lawsonite geochemistry and stability—implication for trace element and water cycles in subduction zones. *J. Metamorph. Geol.* **32**, 455–478 (2014).
72. Usui, T., Kobayashi, K., Nakamura, E. & Helmstaedt, H. Trace element fractionation in deep subduction zones inferred from a lawsonite-eclogite xenolith from the Colorado Plateau. *Chem. Geol.* **239**, 336–351 (2007).
73. Spandler, C., Hermann, J. R., Arculus, R. & Mavrogenes, J. Redistribution of trace elements during prograde metamorphism from lawsonite blueschist to eclogite facies; implications for deep subduction-zone processes. *Contrib. Miner. Pet.* **146**, 205–222 (2003).
74. Zack, T., Foley, S. & Rivers, T. Equilibrium and disequilibrium trace element partitioning in hydrous eclogites (Trescolmen, Central Alps). *J. Pet.* **43**, 1947–1974 (2002).
75. Leat, P. T. et al. Volcanic evolution of the South Sandwich volcanic arc, South Atlantic, from multibeam bathymetry. *J. Volcano. Geotherm. Res* **265**, 60–77 (2013).
76. Miyazaki, T. et al. The first 10 million years of rear-arc magmas following backarc basin formation behind the Izu arc. *Geochem. Geophys. Geosyst.* **21**, e2020GC009114 (2020).
77. Bates, S. L. et al. Barium isotopes reveal role of ocean circulation on barium cycling in the Atlantic. *Geochim. Cosmochim. Acta* **204**, 286–299 (2017).
78. Wolgemuth, K. & Broecker, W. Barium in sea water. *Earth Planet Sci. Lett.* **8**, 372–378 (1970).
79. Foster, D. A., Staubwasser, M. & Henderson, G. M. 226Ra and Ba concentrations in the Ross Sea measured with multicollector ICP mass spectrometry. *Mar. Chem.* **87**, 59–71 (2004).
80. van Zuilen, K., Nägler, T. F. & Bullen, T. D. Barium isotopic compositions of geological reference materials. *Geostand. Geoanal. Res.* **40**, 543–558 (2016).
81. Nan, X. et al. High-precision barium isotope measurements by MC-ICP-MS. *J. Anal. At. Spectrom.* **30**, 2307–2315 (2015).
82. Hart, S. R. & Brooks, C. The geochemistry and evolution of early Precambrian mantle. *Contrib. Miner. Pet.* **61**, 109–128 (1977).
83. Scher, H. D. & Delaney, M. L. Breaking the glass ceiling for high resolution Nd isotope records in early Cenozoic paleoceanography. *Chem. Geol.* **269**, 329–338 (2010).
84. Lugmair, G. & Galer, S. Age and isotopic relationships among the angrites Lewis Cliff 86010 and Angra dos Reis. *Geochim. Cosmochim. Acta* **56**, 1673–1694 (1992).
85. Jackson, M. & Hart, S. Strontium isotopes in melt inclusions from Samoan basalts: implications for heterogeneity in the Samoan plume. *Earth Planet Sci. Lett.* **245**, 260–277 (2006).
86. White, W. M. & Patchett, J. Hf-Nd-Sr isotopes and incompatible element abundances in island arcs: implications for magma origins and crust-mantle evolution. *Earth Planet Sci. Lett.* **67**, 167–185 (1984).
87. Tanaka, T. et al. JNdi-1: a neodymium isotopic reference in consistency with LaJolla neodymium. *Chem. Geol.* **168**, 279–281 (2000).
88. Todt, W., Cliff, R., Hanser, A. & Hofmann, A. Evaluation of a ^{202}Pb-^{205}Pb double spike for high-precision lead isotope analysis. in *Earth Processes: Reading the Isotopic Code, Geophysical Monograph* (eds Basu, A. & Hart, S. R.) Vol. 95, 429–437 (Wiley, 1996).
89. Weis, D. et al. High-precision isotopic characterization of USGS reference materials by TIMS and MC-ICP-MS. *Geochem. Geophys. Geosyst.* **7**, Q08006 (2006).
90. Jochum, K. P. et al. Reference values following ISO guidelines for frequently requested rock reference materials. *Geostand. Geoanal. Res.* **40**, 333–350 (2016).
91. Zindler, A. & Hart, S. Chemical geodynamics. *Annu. Rev. Earth Planet Sci.* **14**, 493–571 (1986).
92. Staudigel, H., Davies, G., Hart, S. R., Marchant, K. & Smith, B. M. Large scale isotopic Sr, Nd and O isotopic anatomy of altered oceanic crust: DSDP/ODP sites 417/418. *Earth Planet Sci. Lett.* **130**, 169–185 (1995).
93. Hauff, F., Hoernle, K. & Schmidt, A. Sr-Nd-Pb composition of Mesozoic Pacific oceanic crust (Site 1149 and 801, ODP Leg 185): implications for alteration of ocean crust and the input into the Izu-Bonin-Mariana subduction system. *Geochem. Geophys. Geosyst.* **4**, 8913 (2003).
94. Bach, W., Peucker-Ehrenbrink, B., Hart, S. R. & Blusztajn, J. S. Geochemistry of hydrothermally altered oceanic crust: DSDP/ODP Hole 504B—implications for seawater-crust exchange budgets and Sr- and Pb-isotopic evolution of the mantle. *Geochem. Geophys. Geosyst.* **4**, 8904 (2003).
95. Ryan, W. et al. Global Multi-Resolution Topography (GMRT) synthesis data set. *Geochem. Geophys. Geosyst.* **10**, Q03014 (2009).
96. Nielsen, S. G. et al. Tracking along-arc sediment inputs to the Aleutian arc using thallium isotopes. *Geochim. Cosmochim. Acta* **181**, 217–237 (2016).

Acknowledgements

We express our gratitude to the WHOI sample repository and the British Antarctic Survey rock archive for providing sediment cores and volcanic samples. This work was funded by Laoshan Laboratory and financially supported by grants from NSF EAR-1829546 to S.G.N. and T.J.H., NSF OCE-2023456 to T.J.H., NSF EAR-1855302 to V.L.R., and NSFC 41903008 to Y.S.

Author contributions

Y.S., S.G.N., V.L.R., and T.J.H. designed the study and selected samples together with D.S.R. and P.T.L. Sample analysis was performed by Y.S., J.B., M.A., and T.J.H. Y.S., S.G.N., and V.L.R. designed the figures and performed data interpretation with input from all co-authors. Y.S. wrote the original draft with input from S.G.N. and V.L.R.; all co-authors reviewed and edited the manuscript.

Competing interests

The authors declare no competing interests.

Additional information

Supplementary information The online version contains supplementary material available at https://doi.org/10.1038/s41467-025-56554-x.

Correspondence and requests for materials should be addressed to Yunchao Shu or Sune G. Nielsen.

Peer review information *Nature Communications* thanks the anonymous, reviewers for their contribution to the peer review of this work. A peer review file is available.